AIP Journal of Applied Physics

Direct current injection and thermocapillary flow for purification of aligned arrays of single-walled carbon nanotubes

Xu Xie, Muhammad A. Wahab, Yuhang Li, Ahmad E. Islam, Bojan Tomic, Jiyuan Huang, Branden Burns, Eric Seabron, Simon N. Dunham, Frank Du, Jonathan Lin, William L. Wilson, Jizhou Song, Yonggang Huang, Muhammad A. Alam, and John A. Rogers

Citation: Journal of Applied Physics **117**, 134303 (2015); doi: 10.1063/1.4916537
View online: http://dx.doi.org/10.1063/1.4916537
View Table of Contents: http://scitation.aip.org/content/aip/journal/jap/117/13?ver=pdfcov
Published by the AIP Publishing

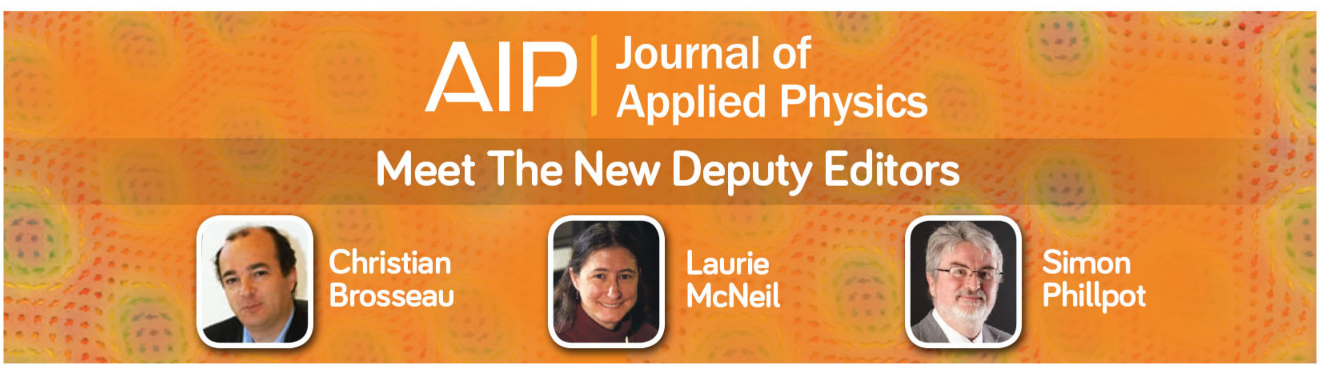

JOURNAL OF APPLIED PHYSICS **117**, 134303 (2015)

Direct current injection and thermocapillary flow for purification of aligned arrays of single-walled carbon nanotubes

Xu Xie,[1] Muhammad A. Wahab,[2] Yuhang Li,[3] Ahmad E. Islam,[1,a)] Bojan Tomic,[4] Jiyuan Huang,[5] Branden Burns,[6] Eric Seabron,[1] Simon N. Dunham,[1] Frank Du,[1] Jonathan Lin,[1] William L. Wilson,[1] Jizhou Song,[7] Yonggang Huang,[8] Muhammad A. Alam,[2] and John A. Rogers[1,b)]

[1]*Department of Materials Science and Engineering, Frederick Seitz Materials Research Laboratory, University of Illinois at Urbana-Champaign, Urbana, Illinois 61801, USA*
[2]*School of Electrical and Computer Engineering, Purdue University, West Lafayette, Indiana 47907, USA*
[3]*Institute of Solid Mechanics, Beihang University, Beijing 100191, China*
[4]*Department of Electrical Engineering, University of Illinois at Urbana-Champaign, Urbana, Illinois 61801, USA*
[5]*Department of Physics, University of Illinois at Urbana-Champaign, Urbana, Illinois 61801, USA*
[6]*Department of Physics, Purdue University, West Lafayette, Indiana 47907, USA*
[7]*Department of Engineering Mechanics and Soft Matter Research Center, Zhejiang University, Hangzhou 310027, China*
[8]*Department of Civil and Environmental Engineering, Department of Mechanical Engineering, Center for Engineering and Health, and Skin Disease Research Center, Northwestern University, Evanston, Illinois 60208, USA*

(Received 10 February 2015; accepted 19 March 2015; published online 7 April 2015)

Aligned arrays of semiconducting single-walled carbon nanotubes (s-SWNTs) represent ideal configurations for use of this class of material in high performance electronics. Development of means for removing the metallic SWNTs (m-SWNTs) in as-grown arrays represents an essential challenge. Here, we introduce a simple scheme that achieves this type of purification using direct, selective current injection through interdigitated electrodes into the m-SWNTs, to allow their complete removal using processes of thermocapillarity and dry etching. Experiments and numerical simulations establish the fundamental aspects that lead to selectivity in this process, thereby setting design rules for optimization. Single-step purification of arrays that include thousands of SWNTs demonstrates the effectiveness and simplicity of the procedures. The result is a practical route to large-area aligned arrays of purely s-SWNTs with low-cost experimental setups. © *2015 AIP Publishing LLC*. [http://dx.doi.org/10.1063/1.4916537]

I. INTRODUCTION

Success in the continued down-scaling of critical dimensions in silicon transistors is largely responsible for the revolutionary changes that have occurred over the last several decades in modern information processing technology. Such scaling becomes increasingly difficult as these dimensions approach fundamental limits.[1] Here, excessive power densities and short channel effects represent two major obstacles.[2,3] One path for further progress involves the development of channel materials that offer superior electrical properties compared to those of silicon. Among the wide variety of materials that can be considered, single-walled carbon nanotubes (SWNTs) remain one of the most promising candidates.[4] Field effect transistors (FETs) built using SWNTs offer superior speeds of operation and levels of energy efficiency compared to those of alternatives; the small dimensions of the SWNTs also allow suppression of short channel effects.[3,5,6] Integration of SWNTs into practical circuits requires large-scale arrays of horizontally aligned, perfectly linear, purely semiconducting SWNTs (s-SWNTs).[3,5] One means to realize such arrays begins with solution processes to purify as-grown mixtures of metallic SWNTs (m-SWNTs) and s-SWNTs,[7,8] followed by alignment of the s-SWNTs via deposition onto a substrate of interest.[9–11] In spite of some notable successes and continued promise,[3,5] key challenges in this scheme include avoiding damage to the SWNTs during solubilization, removing residual surfactant after deposition, and achieving perfect alignment and perfect purity of s-SWNTs (>99.9999%[12]) in the arrays.[5] A different approach, also with some demonstrated utility, begins with growth of chemically and structurally pristine, nearly perfectly aligned SWNTs on quartz substrates,[13,14] followed by removal of the m-SWNTs. Many removal methods, ranging from electrical breakdown[15] to optical ablation[16,17] and chemical etching[18] have been explored, but each has significant disadvantages in terms of efficiency in elimination of m-SWNTs, retention of s-SWNTs and/or applicability to large arrays.[12]

Recently developed purification methods based on nanoscale thermocapillary flows overcome these drawbacks.[19–21] Here, selective, mild heating of m-SWNTs causes temperature gradients that drive local flow of an overcoat of an amorphous small molecule organic material (thermocapillary resist,

a)Present address: Materials and Manufacturing Directorate, Air Force Research Laboratory, Dayton, Ohio 45433, USA.
b)Author to whom correspondence should be addressed. Electronic mail: jrogers@illinois.edu

Tc-resist). Such flows open trenches around the m-SWNTs, thereby exposing them for complete removal by reactive ion etching (RIE). The low temperature operation (several degrees) of this process, together with means for highly selective heating of the m-SWNTs (directly based on their electrical properties), enables unmatched levels of purity, experimentally demonstrated at >99.9925%[20] limited only by the statistics of the measurement and likely much higher. Options for selectively heating of m-SWNTs include electrical probing through partial-gate transistor structures[19] and exposure to electromagnetic waves in the microwave[20] or infrared regimes.[21] These techniques provide excellent selectivity and outstanding performance in purification. The partial-gate transistor structures are, however, cumbersome to fabricate and sometimes leave residues that are difficult to remove. Electromagnetic radiation offers operational simplicity, minimal processing, absence of residue, and scalability, although high throughput operation requires large-scale sources. At the laboratory scale, co-integrated antennas are needed to enhance the microwave fields that can be generated from desktop microwave ovens.[20] For laboratory-scale infrared lasers, exposure requires raster scanning of a small focused spot at rates smaller than 0.4 μm/s.[21] Scale-up is possible, but with capital costs that might lie outside of the realm of resources readily available for academic research.

Here, we introduce an exceptionally simple, alternative thermocapillary based purification approach. Direct current injection using two terminal (2 T) interdigitated electrodes formed with low work-function metals causes Joule heating selectively in the m-SWNTs, with sufficient amplitude to enable thermocapillary flows. Experiments and simulations described in the following highlight the underlying phenomena and provide design guidelines and processing conditions for achieving high purification selectivity and efficiency. Demonstrations involve purifying arrays of thousands of SWNTs in a single step. The scheme represents a practical route to large-area aligned arrays of purely s-SWNTs with readily available experimental setups.

II. PURIFICATION SCHEME

Schematic illustrations shown in Figs. 1(a)–1(d) summarize the overall scheme. First, deposition of Fe catalysts on quartz substrates followed by growth via chemical vapor deposition (CVD) yields horizontally aligned arrays of individual SWNTs (Fig. 1(a)).[14,20] Photolithographic patterning, electron beam evaporation and lift-off of metals with low work-function (smaller than the mid-gap energy of SWNTs ~4.8 eV, Ref. 22) define the interdigitated electrodes (Fig. 1(b)). Thermal evaporation of a thin layer of thermocapillary resist (Tc-resist, typically 30 nm of α,α,α'-Tris(4-hydroxyphenyl)-1-ethyl-4-isopropylbenzene), followed by direct application of pulsed voltages to the electrodes through contacting probe tips causes Joule heating selectively in the m-SWNTs. This mild heating can be sufficient to drive thermocapillary flows in the Tc-resist in the immediate vicinity of the m-SWNTs (Fig. 1(c)).[20,23] Low work-function metals are crucial for such operation. Typically, the electrodes consist of 80 nm Ti (due to the easy evaporation of metal and formation of stable contacts), but other metals

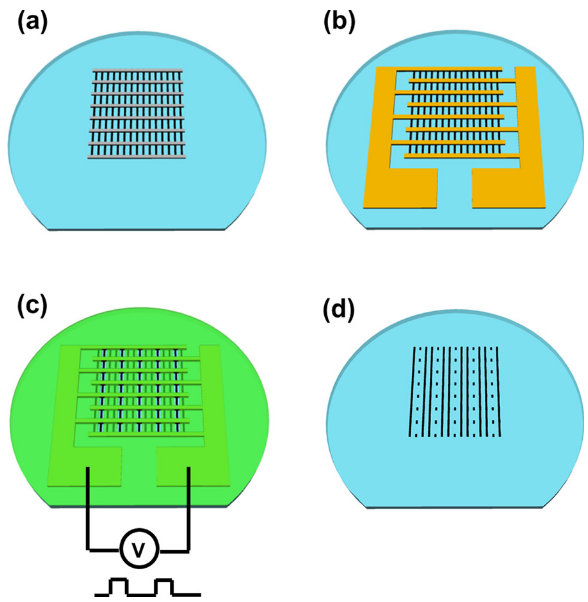

FIG. 1. Schematic illustration of a process for purifying aligned arrays of SWNTs based on direct current injection through two-terminal (2 T) interdigitated electrodes and thermocapillary flows. (a) Growth of SWNTs on quartz substrate by CVD. (b) Fabrication of interdigitated electrodes of low work-function metals. (c) Deposition of a thin layer of Tc-resist, followed by pulsed current injection to induce Joule heating and associated local thermocapillary flows that selectively expose the m-SWNTs. (d) Removal of the exposed m-SWNTs, followed by the Tc-resist and interdigitated electrodes, to leave aligned arrays of purely s-SWNTs.

such as Mo, Al, Mg, etc.[20] can also be used. Here, the Schottky barriers between these metals and the s-SWNTs effectively block the flow of current and thereby avoid any significant Joule heating in (and associated thermocapillary flows around) the s-SWNTs.[20] RIE removes the exposed m-SWNTs, leaving the s-SWNTs unaffected. Finally, removing the Tc-resist with acetone and wet etching the interdigitated electrodes (Transene TFT for Ti) leaves nearly perfectly aligned arrays of linear, pristine, purely s-SWNTs (Fig. 1(d)).

Selectivity and efficiency are important criteria for assessing the operation of this type of purification process.[24] Selectivity demands the elimination of all m-SWNTs and the preservation of most of the s-SWNTs. Efficiency corresponds to the ability to purify large-area arrays of SWNTs rapidly. In addition to the use of low work-function metals as contacts, proper designs of the interdigitated electrodes, carefully selected parameters for inducing the thermocapillary flows, and effective thermal management are important. The following sections highlight these and other essential issues.

III. DESIGN OF INTERDIGITATED ELECTRODES

Schematic illustrations in Fig. 2(a) highlight the important geometric parameters for the interdigitated layout, including the length (L_0) and width (W_0) of the gap between the electrodes, and the length of the electrodes (L_1). Decreasing L_1, while increasing L_0 and W_0 improves the purification efficiency by reducing the unpurified areas (i.e., those occupied by the electrodes). A practical constraint for such scaling, however, is the requirement for

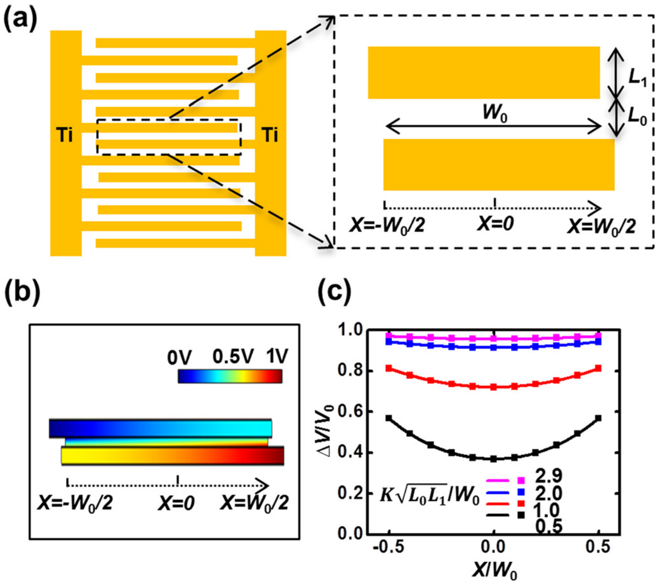

FIG. 2. (a) Schematic illustration of important geometric parameters of the interdigitated electrodes, including the lengths (L_0) and widths (W_0) of the gaps between the electrodes, and the length of the electrode (L_1). (b) FEA of the distribution of electric potential on the interdigitated electrodes. The image is stretched in the direction perpendicular to X axis for ease of viewing. (c) Analytical analysis (solid lines) and FEA (solid squares) of electric potential differences between two adjacent electrodes along the width direction (x-direction), for different designs. When the current transfer length ($K\sqrt{L_0L_1}$, $K=\sqrt{\frac{3r_0t}{4D\rho_0}}$) is larger than W_0, the potential differences approach to the applied voltage (V_0).

spatially uniform heating across the gap (along the width direction). When W_0 is too long or L_1 is too short, the potential drop along the electrodes can be substantial, resulting in non-uniform heating. Such effects can be captured by finite element analysis (FEA, using COMSOL, Inc.) of the distribution of the electrical potential (Fig. 2(b)). Here, the SWNTs are treated as thin film resistors with an equivalent sheet resistance of $r_0/\left(\frac{D}{3}\right)$, where r_0 is the average resistivity of the m-SWNTs ($\sim$50 kΩ/μm),[20] D is the SWNT density (i.e., the number of SWNTs per unit length in the direction perpendicular to their orientation, here taken as 1.5 SWNTs/μm), and the factor of 1/3 originates from the percentage of m-SWNTs in the as-grown arrays.[25] Insulating boundary conditions on the sides of the electrodes ensure periodicity.

An analytical model based on transmission line theory[26] can quantify the role of key parameters in determining the level of uniformity of the electrical potential. The model treats the adjacent electrodes as transmission lines linked by the SWNTs in the channel (as another transmission line). The injected current gradually transfers from one end of the electrode through the SWNTs and into the other. Electrical potential differences between the two electrodes along the width direction (x-direction) can be written

$$\Delta V(x) = \frac{V_0 \cosh(x/L_T)}{\cosh\left(\frac{W_0}{2L_T}\right) + \frac{W_0}{2L_T}\sinh\left(\frac{W_0}{2L_T}\right)}, \qquad (1)$$

where V_0 is the applied voltage, and L_T is the characteristic current transfer length, defined as

$$L_T = \sqrt{\frac{3r_0t}{4D\rho_0}}\sqrt{L_0L_1}. \qquad (2)$$

Here, ρ_0 and t are the resistivity and thickness of the electrodes, respectively. Both the analytical analysis and FEA suggest that increasing L_T/W_0 enhances the uniformity (Fig. 2(c)). Although increasing L_1 or decreasing W_0 achieves this goal, such adjustments reduce the purified area. The preferred option, then, is to increase L_0, which improves both the purification efficiency and the heating uniformity.

IV. RANGE OF VALIDITY FOR SCHOTTKY BARRIERS

Schottky barriers associated with low work-function metals are critically important to good selectivity. Such barriers suppress the flow of current into the s-SWNTs most effectively at small applied biases.[27] Figs. 3(a) and 3(b) show typical experimental measurements and simulated results for 2 T current-voltage (IV) characteristics of arrays of as-grown SWNTs (estimated as $\sim$500 tubes, with the usual mixture of m-SWNTs and s-SWNTs) and purely s-SWNTs (purified by a microwave-based thermocapillary method,[20] estimated as $\sim$333 tubes), respectively. The distances between the electrodes in both cases are 15 μm. Measurements used a vacuum probe-station at room temperature. Simulations assume that 1/3 of the SWNTs are m-SWNTs and that the others are s-SWNT, and that both types have the same diameter distributions.[20] Calculations for the s-SWNTs rely on solving the electrostatics and drift-diffusion transport in a self-consistent manner; the IVs for the m-SWNTs follow from the Landauer formula, with effects of acoustic and optical phonon scattering.[20,28,29] For the as-grown array

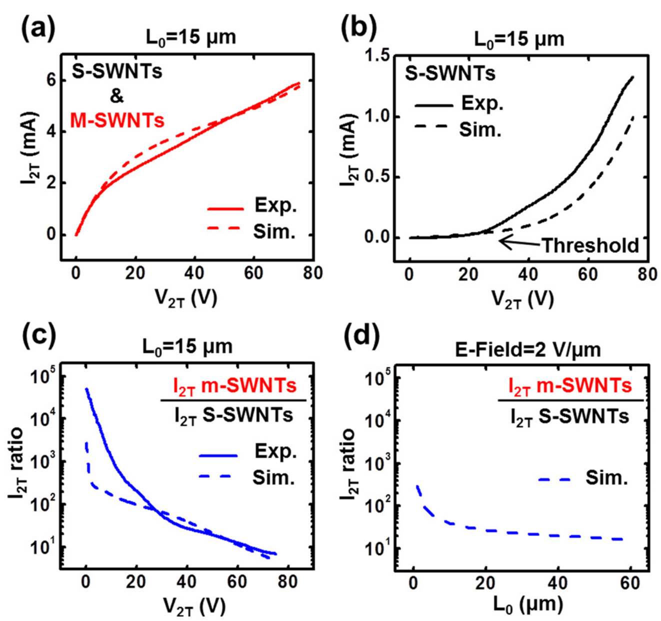

FIG. 3. (a) Representative experimental measurements and simulated results for two terminal (2 T) current-voltage (IV) characteristic of an as-grown array of $\sim$500 SWNTs. (b) Experimental and simulated IV characteristics of an array of purely s-SWNTs ($\sim$333 SWNTs). The current becomes non-negligible for voltages above $\sim$25 V. (c) Ratio of the 2 T current contributed by the m-SWNTs to that from the s-SWNTs as a function of voltage. (d) Ratio of 2 T currents as a function of channel length for an average electric field of 2 V/μm.

(Fig. 3(a)), the total current increases almost linearly with the voltage for voltages <7 V, which is consistent with the dominating contribution of m-SWNTs to the current in this regime. The slope decreases for voltages >7 V, due to increases in phonon scattering. At high voltages, the IV curve becomes sub-linear again, where currents from both m-SWNTs and s-SWNTs contribute in a significant way. This behavior is consistent with the results of Fig. 3(b), which correspond to the case of for purely s-SWNT arrays. Here, the current is negligible at low voltage and then increases dramatically at a threshold voltage of ∼25 V, corresponding to an onset of failure of the Schottky barriers (mainly due to band to band tunneling followed by impact ionization).[28,30] The different IV behaviors for the m-SWNTs and s-SWNTs result in changes in the ratio of their 2 T currents (Fig. 3(c)) with voltage. This ratio gradually decreases from >100 at low voltages (<25 V) to ∼5 at voltages that approach electrical breakdown (75 V). At a fixed bias value, the heating induced in each SWNT is proportional to the current. As a result, the selectivity for heating of the m-SWNT is greatest at low bias values. The conditions for the experiment must be chosen, therefore, to enable thermocapillary flows in this regime.

Further consideration of the selectivity centers on the choice of L_0. For a given electrical field (2 V/μm used in the simulation in Fig. 3(d)), the ratio of currents between the m-SWNTs and s-SWNTs decreases with increasing L_0. Such scaling is mainly attributed to the rise of applied voltages necessary to maintain the electric field at a certain level. We note that the simulations here consider a different measurement condition (air) compared to those in Figs. 3(a)–3(c) (vacuum). However, the overall trends represented in Figure 3 are independent of measurement environment, and the quantitative values are also not affected significantly. Although large L_0 enhances the purification efficiency and the heating uniformity, the selectivity deteriorates if L_0 is too large. In addition, non-bridging SWNTs may appear for increased L_0. Thus, there is a trade-off in optimizing L_0.

V. PULSED HEATING FOR THERMAL MANAGEMENT

Thermal management is important, particularly when applied to large numbers of SWNTs where increases in the background temperature associated with heating of the SWNTs, in aggregate, can be non-negligible. This increase in temperature reduces the viscosity of the Tc-resist, thereby changing the dynamics of thermocapillary flows in a manner that can be difficult to control, particularly in samples that involve significant spatial variations in the density of the SWNTs. The effects of cumulative heating can be minimized by the use of pulsed applied voltages, with duty cycles sufficiently small to allow cooling in between pulses. Three dimensional (3D) FEA (ABAQUS) reveals the effects and aids in optimization. Fig. 4(a) shows a schematic representation of the 3D layouts used for simulations that consider, for simplicity, heating only in the m-SWNTs. The calculations use periodic boundary conditions with arrays of m-SWNTs that have lengths of 15 μm and spacings that depend on the density (assuming that 1/3 of the SWNTs are metallic). As shown in Fig. 4(a), the m-SWNTs lie beneath a layer of

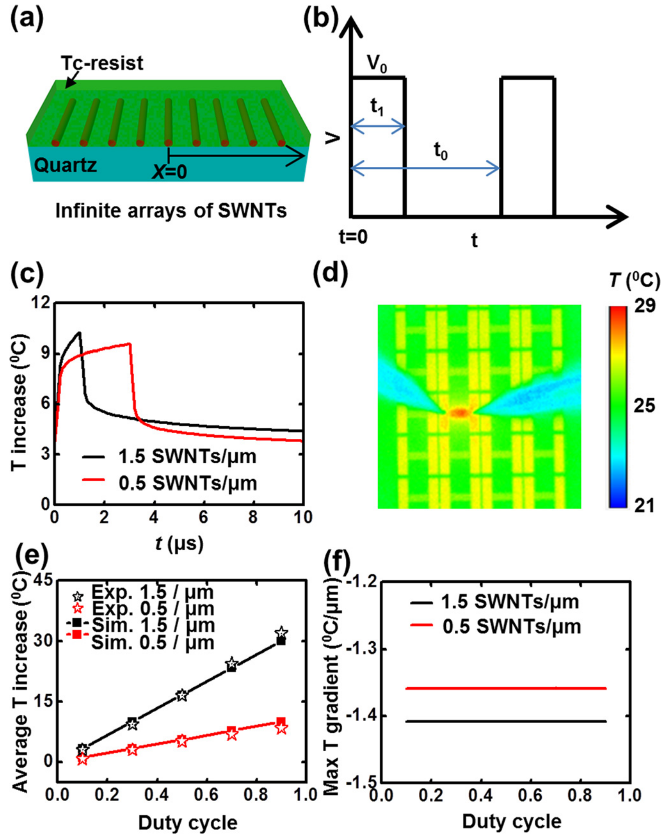

FIG. 4. (a) Schematic representation of the 3D structure used for temperature calculations. (b) Illustration of the key parameters of the applied pulsed voltage, including the length of the pulse t_1 and the interval between pulses t_0. (c) Simulated temperature increase of the top surface of the Tc-resist (at x = 0) as a function of time within a heating cycle. The black curve corresponds to an array density of 1.5 SWNTs/μm, with $t_0 = 10\,\mu s$ and $t_1 = 1\,\mu s$. The red curve corresponds to an array density of 0.5 SWNTs/μm, with $t_0 = 10\,\mu s$ and $t_1 = 3\,\mu s$. (d) Infrared camera image of an array during application of pulsed voltage. (e) Experimental measurements and simulated results for the temperature increase during application of pulsed voltages with different duty cycles. The results show a linear relationship between the temperature rise and the duty cycle. (f) Simulated results for the maximum temperature gradient as a function of duty cycle.

Tc-resist with a thickness of 30 nm on a quartz substrate (500 μm thick). The thermal conductivity, density, and heat capacity are 0.2 W·m^{-1}·K^{-1}, 1160 kg·m^{-3}, and 1500 J·kg^{-1}·K^{-1} for the Tc-resist; 4000 W·m^{-1}·K^{-1}, 1300 kg·m^{-3}, and 400 J·Kg^{-1}·K^{-1} for the m-SWNT; and 6 W·m^{-1}·K^{-1}, 2650 kg·m^{-3}, and 740 J·Kg^{-1}·K^{-1} for quartz.[19,31,32] The top surface of the Tc-resist layer is assumed to be adiabatic.[19,33] The bottom of the quartz substrate has a temperature fixed to the ambient.

Fig. 4(b) illustrates the key parameters of the pulsed bias, including the pulse width t_1 and repetition period t_0. Their ratio defines the duty cycle. An applied voltage $V_0 = 25$ V yields an average power density of 19.5 W/m (estimated from experiments) per m-SWNT. Simulations involve $t_0 = 10\,\mu s$, and various duty cycles and densities of SWNTs to reveal their effects on the temperature increases and associated gradients. Fig. 4(c) shows the temperature increase at the top surface of the Tc-resist (at x = 0) as a function of time within a single pulse cycle. The black and red curves correspond to arrays with densities of 1.5

SWNTs/μm (duty cycle = 10%) and 0.5 SWNTs/μm (duty cycle = 30%), respectively. The temperatures continuously rise within the duration of the pulse and immediately begin to decrease at the end of the pulse. Decreasing the duty cycle or the density of the SWNTs reduces the cumulative increase in temperature. An infrared camera (FLIR A655sc) allows experimental measurements for comparison to these simulation results. Fig. 4(d) shows an infrared image of an array during application of a pulsed voltage. The red region in between the tips results from elevated temperatures due to cumulative heating associated with SWNTs in this area. Fig. 4(e) summarizes experimental measurements and simulated results for increases in temperature for different duty cycles. The experimental data correspond to analysis of the infrared images, calibrated based on measurements using the same devices heated to well-defined temperatures on a hotplate. The computed temperature rise corresponds to an average over the unit cell and over a period of time. The resolution of the camera (~35 μm) is much larger than the spacings between the SWNTs (~1 μm); likewise, the time response (20 ms) is much longer than the duration of a single pulse (10 μs). As expected, increases in tube density lead to increases in temperature. The measured and simulated results indicate a linear increase in the temperature with the duty cycle, as might be expected. Decreasing the duty cycle only decreases the cumulative temperature rise. The temperature gradients, which determine the thermocapillary stresses that drive flow in the Tc-resist, are independent of duty cycle (Fig. 4(f)). These results confirm that controlling the duty cycle represents an important means for the thermal management.

Besides the thermal management, one may also expect that pulse mode heating could help to reduce the trench widths, which is critical for processing high density arrays of SWNTs. However, experimentally observed trench widths with pulsed heating are comparable to those from DC heating (~200 nm). This result most likely follows from the relative long pulse duration used in the experiment. For a pulse width of 1 μs (shortest pulse duration provided by the pulse generator), the thermal diffusion length in the quartz substrate and the Tc-resist are around 3.6 μm and 600 nm, respectively. Both of those lengths are larger than the typical trench widths. Therefore, although pulse heating helps to constrain the heat spreading, the pulse durations explored here are too long to affect the trench width.

VI. DEMONSTRATIONS OF PURIFICATION

Selectivity and efficiency are influenced by materials choices (the low work-function metal contacts), interdigitated electrodes designs (L_0, W_0, L_1), and operation conditions (V_0, pulse width and duty cycles, background heating). A wide range of combinations of these parameters enable proper operation of the purification process. Demonstrations involve arrays of thousands of SWNTs (with densities ~0.5 SWNTs/μm or ~1.5 SWNTs/μm). Fig. 5(a) shows an optical image of interdigitated electrodes of Ti (80 nm thick), with $L_0 = 15\,\mu$m, $W_0 = 500\,\mu$m, and $L_1 = 30\,\mu$m, and 4 parallel channels. The current transfer length $L_T = 2.9W_0$ yields

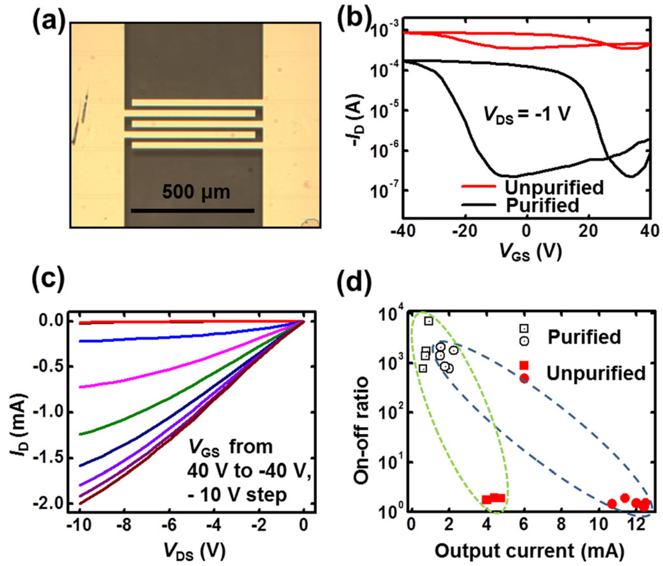

FIG. 5. (a) Optical image of a small set of interdigitated electrodes. (b) Representative transfer characteristics of transistors based on purified (black) and unpurified (red) arrays of SWNTs ones. The density before the purification is ~1.5 SWNTs/μm. (c) Typical output characteristics of the transistor that uses purified SWNT arrays. (d) Statistical results of the on-off ratio and output current for transistors based on purified and unpurified arrays. The green and blue dashed ellipses indicate results from SWNTs with density ~ 0.5 SWNTs/μm and ~1.5 SWNTs/μm, respectively.

uniform electric potentials (Fig. 2(c)). Applying a pulsed voltage of 25 V provides sufficient temperature gradients to induce thermocapillary flow, while maintaining the effectiveness of Schottky barriers for selective heating. The pulse period is 10 μs, applied for a total time of 15 min. Duty cycles of 30% and 10% proved effective for arrays with densities of ~0.5 SWNTs/μm and 1.5 SWNTs/μm, respectively. These choices not only minimize cumulative heating but also allow sufficient time for the full formation of trenches. This process occurs inside a vacuum probe-station, with a heating stage that provides a uniform background temperature of 80 °C, thereby reducing the viscosity of the Tc-resist to facilitate the thermocapillary flow. Other procedures, such as RIE etching of the m-SWNTs and wet etching of the electrodes, follow procedures reported previously.[19–21] Transistors formed using arrays of SWNTs purified in this case use source and drain contacts of Ti (1 nm)/Pd (80 nm) formed at positions that coincide with those of the removed Ti interdigitated electrodes. Layers of PMMA (950 A7, 1500 rpm for 45 s and 4000 rpm for 30 s, baking 110 °C for 8 min) and Ti (50 nm) serve as the gate dielectrics and gate electrodes, respectively. Fig. 5(b) shows typical transfer characteristics for transistors based on purified and unpurified SWNT arrays (density ~ 1.5 SWNTs/μm). Fig. 5(c) gives representative output characteristics of a transistor based on a purified array. Purification increases the on-off ratio from 2.5 to ~10^3, consistent with the removal of all m-SWNTs. At the same time, the on current drops to ~20% of the value before purification. The loss in current is somewhat larger than that achieved on small arrays of SWNTs using previous approaches[19] but lies within the range observed in mm-scale arrays.[19] The discrepancy might arise from slight overetching (95 W in plasma etching power compared to 80 W used previously), during the removal of the m-SWNTs. Statistical results of the transistor studies appear in Fig. 5(d). The green and blue dashed ellipses correspond to arrays with densities ~ 0.5 SWNTs/μm and ~ 1.5 SWNTs/μm, respectively. The on-off ratios range from 0.76×10^3 to 6.9×10^3 after purification, and the output current retention ranges from 15% to 22%.

VII. CONCLUSIONS

In conclusion, this paper presents a simple scheme for purifying arrays of SWNTs based on selective thermocapillary effects that arise from direct current injection using interdigitated electrodes. The method is effective and scalable, and can be implemented easily. Although the densities of SWNTs that can be processed effectively in this way are limited by the widths of the trenches that form from thermocapillary flow (<5 SWNTs/μm,[19,34] for the Tc-resist used here) the resulting large-area aligned arrays of purely s-SWNTs are sufficient for many applications and studies of thin film transistors,[12] radio frequency low noise amplifiers,[35] sensors,[36] and other devices.[29] Multiple transfer printing of purified arrays, or use on arrays with high density, enriched content of s-SWNTs (from CVD growth[37,38] or solution process[10]) represent promising paths to reach the ultimate goals (density > 125 SWNTs/μm and purity > 99.9999%) associated with applications in digital electronics.[12]

ACKNOWLEDGMENTS

We thank Jeffery Grau for making photomasks. Experiments were carried out in part in the Frederick Seitz Materials Research Laboratory Central Research Facilities, University of Illinois at Urbana-Champaign. This work was funded by NSF (CMMI 14-36133 GOALI). The Purdue group acknowledges computational resources from Network of Computational Nanotechnology and the financial support from the NCN-NEEDS program, which is funded by the National Science Foundation, contract 1227020-EEC, and by the Semiconductor Research Corporation.

1. See http://www.itrs.net for ITRS ERM, 2013.
2. E. Pop, S. Sinha, and K. E. Goodson, Proc. IEEE **94**, 1587 (2006).
3. G. S. Tulevski, A. D. Franklin, D. Frank, J. M. Lobez, Q. Cao, H. Park, A. Afzali, S. J. Han, J. B. Hannon, and W. Haensch, ACS Nano **8**, 8730 (2014).
4. P. Avouris, Z. Chen, and V. Perebeinos, Nat. Nanotechnol. **2**, 605 (2007).
5. Q. Cao and S. J. Han, Nanoscale **5**, 8852 (2013).
6. A. D. Franklin, M. Luisier, S. J. Han, G. Tulevski, C. M. Breslin, L. Gignac, M. S. Lundstrom, and W. Haensch, Nano Lett. **12**, 758 (2012).
7. M. S. Arnold, A. A. Green, J. F. Hulvat, S. I. Stupp, and M. C. Hersam, Nat. Nanotechnol. **1**, 60 (2006).
8. H. Liu, D. Nishide, T. Tanaka, and H. Kataura, Nat. Commun. **2**, 309 (2011).
9. H. Park, A. Afzali, S. J. Han, G. S. Tulevski, A. D. Franklin, J. Tersoff, J. B. Hannon, and W. Haensch, Nat. Nanotechnol. **7**, 787 (2012).
10. Q. Cao, S. Han, and G. S. Tulevski, Nat. Commun. **5**, 5071 (2014).
11. Q. Cao, S. Han, G. S. Tulevski, Y. Zhu, D. Lu, and W. Haensch, Nat. Nanotechnol. **8**, 180 (2013).
12. A. D. Franklin, Nature **498**, 443 (2013).
13. C. Kocabas, S. H. Hur, A. Gaur, M. A. Meitl, M. Shim, and J. A. Rogers, Small **1**, 1110 (2005).
14. J. Xiao, S. Dunham, P. Liu, Y. Zhang, C. Kocabas, L. Moh, Y. Huang, K. Hwang, C. Lu, W. Huang, and J. A. Rogers, Nano Lett. **9**, 4311 (2009).
15. A. Liao, R. Alizadegan, Z. Ong, S. Dutta, F. Xiong, K. Hsia, and E. Pop, Phys. Rev. B **82**, 205406 (2010).
16. M. Mahjouri-Samani, Y. Zhou, W. Xiong, Y. Gao, M. Mitchell, and Y. Lu, Nanotechnology **20**, 495202 (2009).
17. H. C. Shim, J. Song, Y. K. Kwak, S. Kim, and C. Han, Nanotechnology **20**, 065707 (2009).
18. G. Zhang, P. Qi, X. Wang, Y. Lu, X. Li, R. Tu, S. Bangsaruntip, D. Mann, L. Zhang, and H. Dai, Science **314**, 974 (2006).
19. S. H. Jin, S. N. Dunham, J. Song, X. Xie, J. H. Kim, C. Lu, A. Islam, F. Du, J. Kim, J. Felts, Y. Li, F. Xiong, M. A. Wahab, M. Menon, E. Cho, K. L. Grosse, D. J. Lee, H. U. Chung, E. Pop, M. A. Alam, W. P. King, Y. Huang, and J. A. Rogers, Nat. Nanotechnol. **8**, 347 (2013).
20. X. Xie, S. H. Jin, M. A. Wahab, A. E. Islam, C. Zhang, F. Du, E. Seabron, T. Lu, S. N. Dunham, H. I. Cheong, Y. C. Tu, Z. Guo, H. U. Chung, Y. Li, Y. Liu, J. H. Lee, J. Song, Y. Huang, M. A. Alam, W. L. Wilson, and J. A. Rogers, Nat. Commun. **5**, 5332 (2014).
21. F. Du, J. R. Felts, X. Xie, J. Song, Y. Li, M. R. Rosenberger, A. E. Islam, S. H. Jin, S. N. Dunham, C. Zhang, W. L. Wilson, Y. Huang, W. P. King, and A. J. A. Rogers, ACS Nano **8**, 12641 (2014).
22. P. Liu, Q. Sun, F. Zhu, K. Liu, K. Jiang, L. Liu, Q. Li, and S. Fan, Nano Lett. **8**, 647 (2008).
23. S. H. Jin, S. N. Dunham, J. Z. Song, X. Xie, J. H. Kim, C. F. Lu, A. Islam, F. Du, J. Kim, J. Felts, Y. H. Li, F. Xiong, M. A. Wahab, M. Menon, E. Cho, K. L. Grosse, D. J. Lee, H. U. Chung, E. Pop, M. A. Alam, W. P. King, Y. G. Huang, and J. A. Rogers, Nat. Nanotechnol. **8**, 347 (2013).
24. M. C. Hersam, Nat. Nanotechnol. **3**, 387 (2008).
25. A. E. Islam, F. Du, X. Ho, S. H. Jin, S. Dunhamn, and J. A. Rogers, J. Appl. Phys. **111**, 054511 (2012).
26. H. H. Berger, Solid State Electron. **15**, 145 (1972).
27. J. Svensson and E. E. B. Campbell, J. Appl. Phys. **110**, 111101 (2011).
28. M. A. Wahab, S. H. Jin, A. E. Islam, J. Kim, J. H. Kim, W. H. Yeo, D. J. Lee, H. U. Chung, J. A. Rogers, and M. A. Alam, ACS Nano **7**, 1299 (2013).
29. X. Xie, A. E. Islam, M. A. Wahab, L. Ye, X. Ho, M. A. Alam, and J. A. Rogers, ACS Nano **6**, 7981 (2012).
30. A. Liao, Y. Zhao, and E. Pop, Phys. Rev. Lett. **101**, 256804 (2008).
31. S. H. Jin, A. E. Islam, T. I. Kim, J. H. Kim, M. A. Alam, and J. A. Rogers, Adv. Funct. Mater. **22**, 2276 (2012).
32. D. Klimenta, S. Nikolajevic, and M. Sredojevic, Eur. Trans. Electron. Power **17**, 427 (2007).
33. X. Xie, K. L. Grosse, J. Song, C. Lu, S. Dunham, F. Du, A. E. Islam, Y. Li, Y. Zhang, E. Pop, Y. Huang, W. P. King, and J. A. Rogers, ACS Nano **6**, 10267 (2012).
34. S. H. Jin, J. Song, H. U. Chung, C. Zhang, S. N. Dunham, X. Xie, F. Du, T. I. Kim, J. H. Lee, Y. Huang, and J. A. Rogers, J. Appl. Phys. **115**, 054315 (2014).
35. J. E. Baumgardner, A. A. Pesetski, J. M. Murduck, J. X. Przybysz, J. D. Adam, and H. Zhang, Appl. Phys. Lett. **91**, 052107 (2007).
36. M. E. Roberts, M. C. LeMieux, and Z. Bao, ACS Nano **3**, 3287 (2009).
37. J. Li, K. Liu, S. Liang, W. Zhou, M. Pierce, F. Wang, L. Peng, and J. Liu, ACS Nano **8**, 554 (2014).
38. Y. Che, C. Wang, J. Liu, B. Liu, X. Lin, J. Parker, C. Beasley, H. S. Wong, and C. Zhou, ACS Nano **6**, 7454 (2012).